CHAPTER 9

Numerical Simulation of Limit Order Books

9.1 Introduction

This chapter describes useful algorithms and their implementations for the numerical simulation of limit order books. The basic algorithm simulating a zero-intelligence limit order book is presented, and then extended to the case of a multivariate Hawkes process-driven order book. Numerical results are analyzed, and compared to empirical data.

9.2 Zero-intelligence Limit Order Book Simulator

9.2.1 An algorithm for Poissonian order flows

We describe a basic algorithm for the simulation of the limit order book model of Chapters 6 and 7. We will assume for notational simplicity that the order book is symmetric, i.e. that the intensities of arrival of orders of various types are identical on the bid and ask side. We can thus drop the ± signs of our notations, and define here with obvious notations:

$$\lambda^L = \left(\lambda_1^L, \ldots, \lambda_K^L\right),$$

$$\Lambda^L = \sum_{i=1}^{K} \lambda_i^L,$$

$$\lambda^C(\mathbf{a}) = \left(\lambda_1^C a_1, \ldots, \lambda_K^C a_K\right),$$

$$\Lambda^C(\mathbf{a}) = \sum_{i=1}^{K} \lambda_i^C a_i,$$

$$\lambda^C(\mathbf{b}) = \left(\lambda_1^C|b_1|, \ldots, \lambda_K^C|b_K|\right),$$

$$\Lambda^C(\mathbf{b}) = \sum_{i=1}^{K} \lambda_i^C|b_i|,$$

$$\Lambda(\mathbf{a},\mathbf{b}) = 2(\lambda^M + \Lambda^L) + \Lambda^C(\mathbf{a}) + \Lambda^C(\mathbf{b}).$$

Using these notations, the routine for the simulation of the limit order book is sketched in Algorithm 1 [see also Gatheral and Oomen (2010) for a similar description].

Algorithm 1 Order book simulation with Poisson order flows.

Require: *Model parameters*: K (number of visible limits), $\lambda^M, \{\lambda_i^L\}_{i\in\{1,\ldots K\}}, \{\lambda_i^C\}_{i\in\{1,\ldots K\}}$ (intensities of order flows), a_∞, b_∞ (size of hidden limits), random distributions $\mathcal{V}_L, \mathcal{V}_M, \mathcal{V}_C$ (volume of limit, market and cancel orders).

Simulation Parameters: N (length of simulation in event time), $\mathbf{X}_{\text{init}}$ (initial state of the limit order book)

1: **Initialization**: Set $t \leftarrow 0$ (physical time), $\mathbf{X}(0) \leftarrow \mathbf{X}_{\text{init}}$.

2: **for** $n = 1, \ldots, N$

3: **Update the cancellation intensities**: $\Lambda^C(\mathbf{b}) = \sum_{i=1}^K \lambda_i^C|b_i|$, $\Lambda^C(\mathbf{a}) = \sum_{i=1}^K \lambda_i^C a_i$..

4: **Time of next event**: Draw the waiting time τ from an exponential distribution with parameter $\Lambda(\mathbf{a},\mathbf{b}) = 2(\lambda^M + \Lambda^L) + \Lambda^C(\mathbf{a}) + \Lambda^C(\mathbf{b})$.

5: **Type of next event**: Draw an event type according to the probability vector $\left(\lambda^M, \lambda^M, \Lambda^L, \Lambda^L, \Lambda^C(\mathbf{a}), \Lambda^C(\mathbf{b})\right)/\Lambda(\mathbf{a},\mathbf{b})$. These probabilities correspond respectively to a buy market order, a sell market order, a buy limit order, a sell limit order, a cancellation of an existing sell order and a cancellation of an existing buy order.

6: **Volume of next event**: Depending on the event type, draw the order volume from one of the random distributions $\mathcal{V}_L, \mathcal{V}_M, \mathcal{V}_C$.

7: **Price of next event**:

8: **if** the next event is a limit order **then**

9: Draw the relative price level according to the probability vector $\left(\lambda_1^L, \ldots, \lambda_K^L\right)/\Lambda^L$.

10: **end if**

11: **if** the next event is a cancellation **then**

Contd...

Algorithm 1 Order book simulation with Poisson order flows.

12: Draw the relative price level at which to cancel an order from according to the probability vector $\left(\lambda_1^C a_1, \ldots, \lambda_K^C a_K\right) / \Lambda^C(\mathbf{a})$ (ask case) or $\left(\lambda_1^C |b_1|, \ldots, \lambda_K^C |b_K|\right) / \Lambda^C(\mathbf{b})$ (bid case).

13: **end if**

14: Set $t \leftarrow t + \tau$ and **update the order book** according to the new event.

15: **Enforce the boundary conditions**: $a_i \leftarrow a_\infty$, $i \geq K+1$ and $b_i \leftarrow b_\infty$, $i \geq K+1$.

16: **end for**

This algorithm is simply the transcription of the limit order book modelled in Chapter 6, enhanced as in Chapter 7 to allow random sizes of submitted orders of all types. This feature will help producing more realistic simulated data.

9.2.2 Parameter estimation

The parameters of the model are estimated on the dataset presented in Appendix B.6. In this section we analyze the results computed with the parameters estimated for the stock SCHN.PA (Schneider Electric) in March 2011. These results and figures are given as illustration, but it is important to note that they are qualitatively similar for all CAC 40 stocks.

Let T be the length of the time window of interest each day. If N_T^M is the total number of trades (buy and sell) during this time window, then the estimate for the intensity of the market orders is

$$\widehat{\lambda^M} = \frac{N_T^M}{2T}.$$

If $N_{i,T}^L$ is the total number of limit orders (buy and sell) submitted i ticks away from the best opposite quote during the time interval of length T, then the estimate for the intensity of the limit orders i ticks away from the best opposite quote is

$$\widehat{\lambda_i^L} = \frac{N_{i,T}^L}{2T}.$$

As for the cancellation intensities, we need to normalize the count by the (temporal) average number of shares $\langle \mathbf{X}_i \rangle$ at distance i from the best opposite quote. If $N_{i,T}^C$ is the total number of cancellation orders (buy and sell) submitted i ticks away from the best opposite quote during the time interval of length T, then the estimate for the intensity of the cancellation orders i ticks away from the best opposite quote is

$$\widehat{\lambda_i^C} = \frac{1}{\langle \mathbf{X}_i \rangle} \frac{N_{i,T}^C}{2T}$$

We then average $\widehat{\lambda^M}$, $\widehat{\lambda_i^L}$ and $\widehat{\lambda_i^L}$ across 23 trading days to get the final estimates. As for the volumes, we compute the empirical distributions of the volumes for each type of orders, and we fit by maximum likelihood estimation a log-normal distribution with parameters $(\widehat{v^M}, \widehat{s^M})$ (market orders), $(\widehat{v^L}, \widehat{s^L})$ (limit orders) and $(\widehat{v^C}, \widehat{s^C})$ (cancellation orders).

The parameters estimated for SCHN.PA in March 2011 are summarized in Tables 9.1 and 9.2. A graphic representation of these parameters is given in Fig. 9.1 and Fig. 9.2.

Table 9.1 Model parameters for the stock SCHN.PA (Schneider Electric) in March 2011 (23 trading days). Figures 9.1 and 9.2 are graphical representation of these parameters

K	30
a_∞	250
b_∞	250
(v^M, s^M)	$(4.00, 1.19)$
(v^L, s^L)	$(4.47, 0.83)$
(v^C, s^C)	$(4.48, 0.82)$
$\lambda^{M^\pm}$	0.1237

Table 9.2 Model parameters for the stock SCHN.PA (Schneider Electric) in March 2011 (23 trading days). Figures 9.1 and 9.2 are graphical representation of these parameters

i (ticks)	$\langle \mathbf{X}_i \rangle$ (shares)	$\lambda_i^{L^\pm}$	$10^3.\lambda_i^{C^\pm}$
1	276	0.2842	0.8636
2	1129	0.5255	0.4635
3	1896	0.2971	0.1487
4	1924	0.2307	0.1096
5	1951	0.0826	0.0402
6	1966	0.0682	0.0341

Contd...

i (ticks)	$\langle \mathbf{X}_i \rangle$ (shares)	$\lambda_i^{L^\pm}$	$10^3.\lambda_i^{C^\pm}$
7	1873	0.0631	0.0311
8	1786	0.0481	0.0237
9	1752	0.0462	0.0233
10	1691	0.0321	0.0178
11	1558	0.0178	0.0127
12	1435	0.0015	0.0012
13	1338	0.0001	0.0001
14	1238	0.0	0.0
15	1122	⋮	⋮
16	1036		
17	943		
18	850		
19	796		
20	716		
21	667		
22	621		
23	560		
24	490		
25	443		
26	400		
27	357		
28	317		
29	285	⋮	⋮
30	249	0.0	0.0

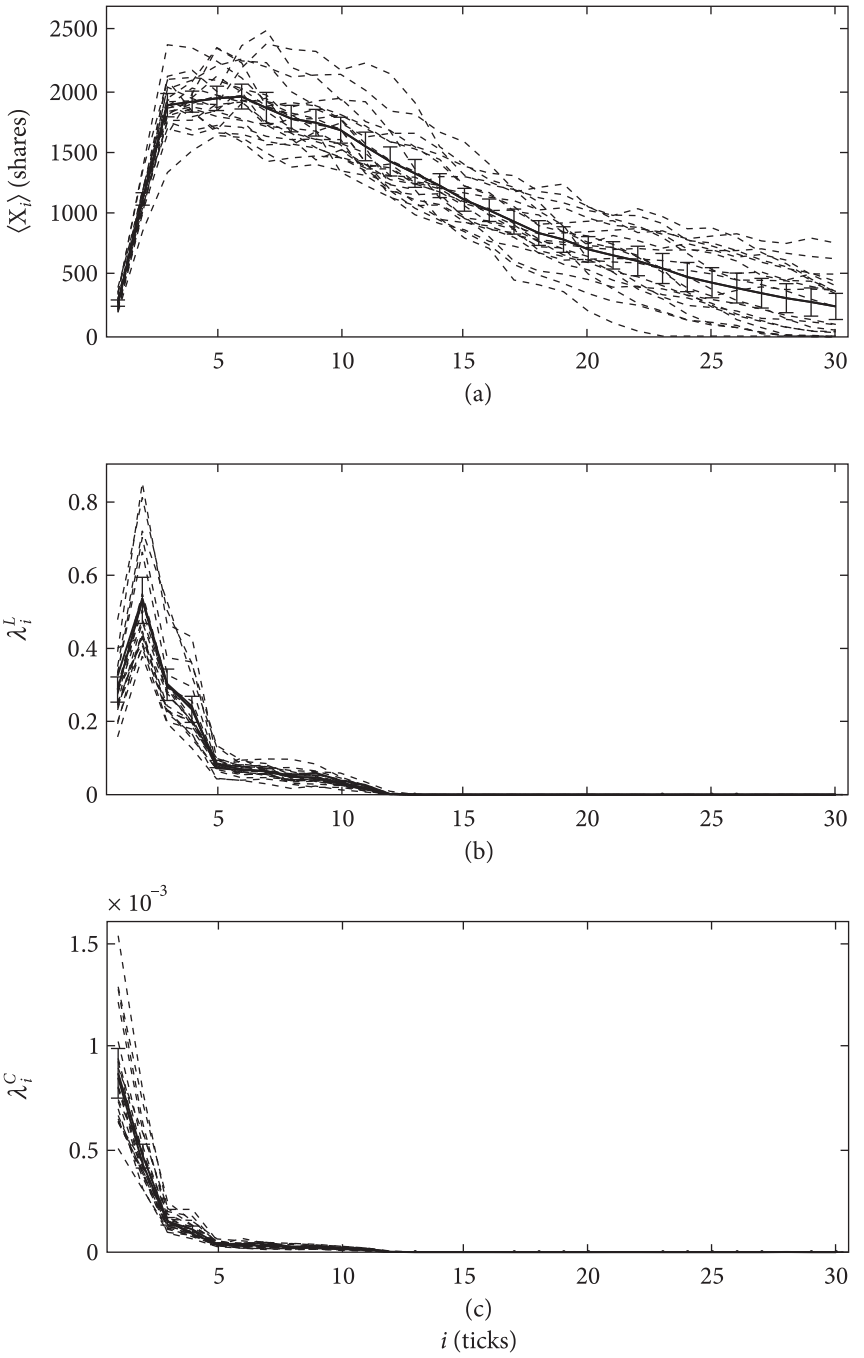

Fig. 9.1 Model parameters: Arrival rates and average depth profile (parameters as in Table 9.2). Error bars indicate variability across different trading days. Extracted from Abergel and Jedidi (2013)

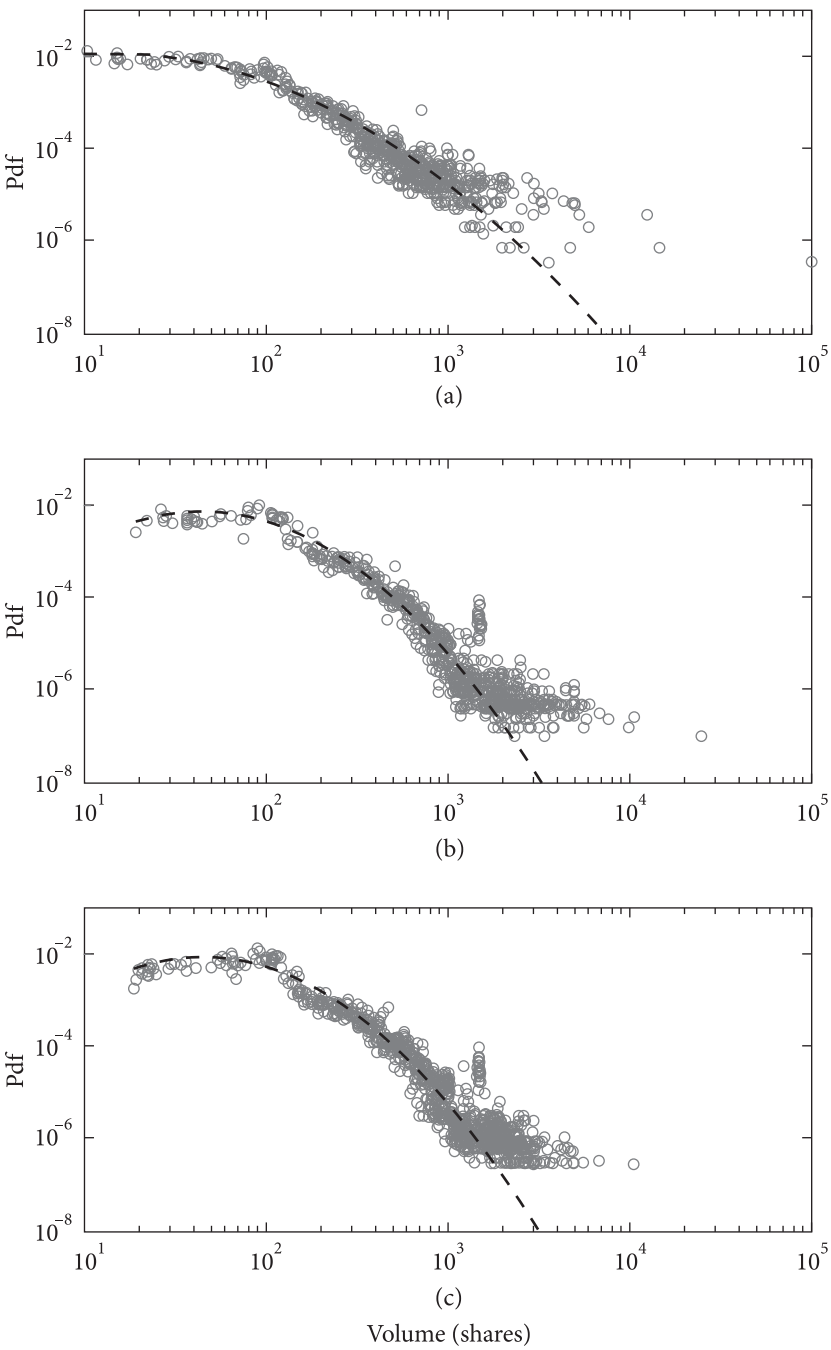

Fig. 9.2 Model parameters: Volume distribution. Panels $(a), (b)$ and (c) correspond respectively to market, limit and cancellation orders volumes. Dashed lines are lognormal fits (parameters as in Table 9.1). Extracted from Abergel and Jedidi (2013)

9.2.3 Performances of the simulation

We compute on our simulated data several quantities of interest. Figure 9.3 represents the average shape of the order book. Recall that this shape has been analytically determined in Chapter 7 in the case of a one-sided model. The agreement between the simulated shape and the empirical one is fairly good. A cross-sectional view of this quantity for all CAC 40 stocks is provided in the next subsection (Fig. 9.10 Panel (a)).

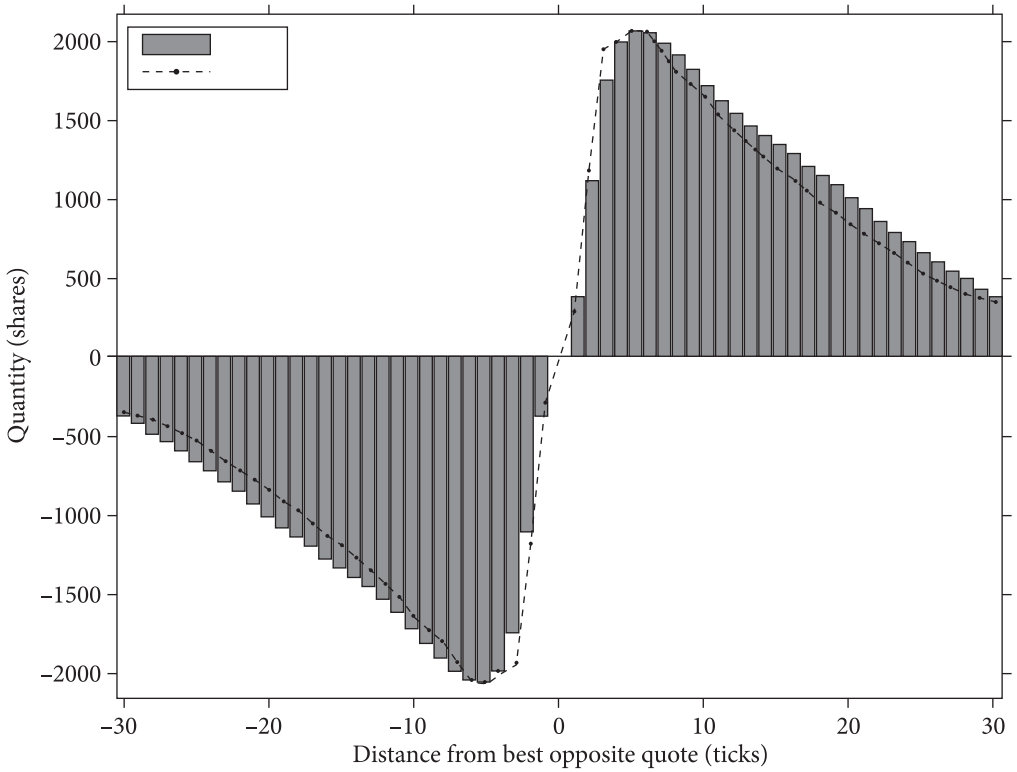

Fig. 9.3 Average depth profile. Simulation parameters are summarized in Tables 9.1 and 9.2. Extracted from Abergel and Jedidi (2013)

We also study some properties of the price process derived from the order book simulations. The distribution of the spread is given in Fig. 9.4. We observe that the simulated distribution is *tighter* than the empirical one. This observation stands for all CAC 40 stocks, as documented Fig. 9.10 Panel (b). It must however be taken with a grain of salt, as the spread distribution is highly sensitive to many parameters of the model. In Section 9.3, we present a qualitative study of the spread distribution under various modelling assumptions for the arrival of orders.

Figure 9.5 shows the fast decay of the autocorrelation function of the price increments. Note the high negative autocorrelation of simulated trade prices relatively to the data. This feature is most likely due to the fact that we have assumed a symmetric order book and Poissonian arrival of orders: In real markets, order splitting induces a clustering of market orders of identical signs, so that the traded prices in a sequence of market orders are closer to one another that in the zero-intelligence case for which the *bid-ask bounce* effect[1] is important.

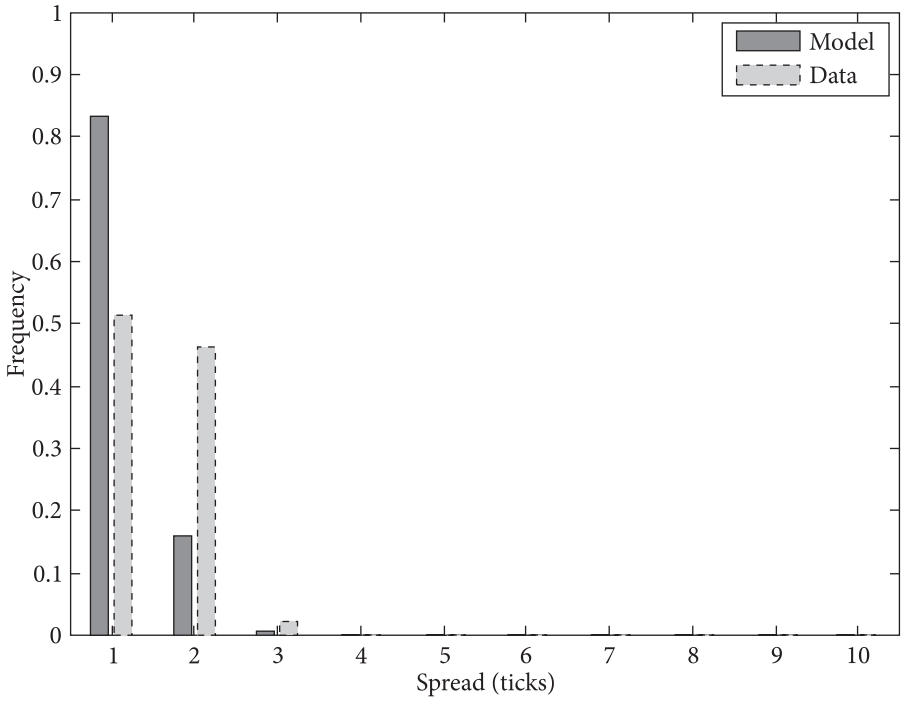

Fig. 9.4 Probability distribution of the spread. Note that the model (dark gray) predicts a tighter spread than the data. Extracted from Abergel and Jedidi (2013)

Figure 9.6 gives an example of simulated path for the mid-price. Figure 9.7 plots the histogram of the empirical distribution of the price increments over 1000 events. At this (large) scale, the normal distribution is a good match. This is a well-known observation, called asymptotic normality of price increments. Figure 9.8 shows the Q-Q plots of the mid-price increments for four different scales, from 1 second to 5 minutes. The convergence of the distribution of the price increments towards a Gaussian distribution as the time scale of observation increases is clearly observed.

[1]The bid-ask bounce effect describes the fact that the signs of market orders generally alternate, thereby creating a large change in traded prices due to the presence of the bid-ask spread

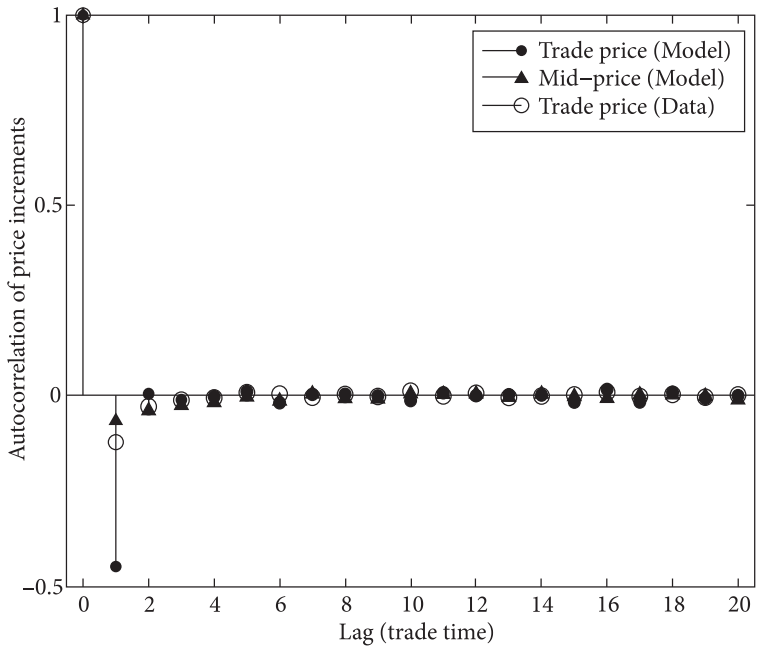

Fig. 9.5 Autocorrelation of price increments. This figure shows the fast decay of the autocorrelation function, and the large negative autocorrelation of trades at the first lag. Extracted from Abergel and Jedidi (2013)

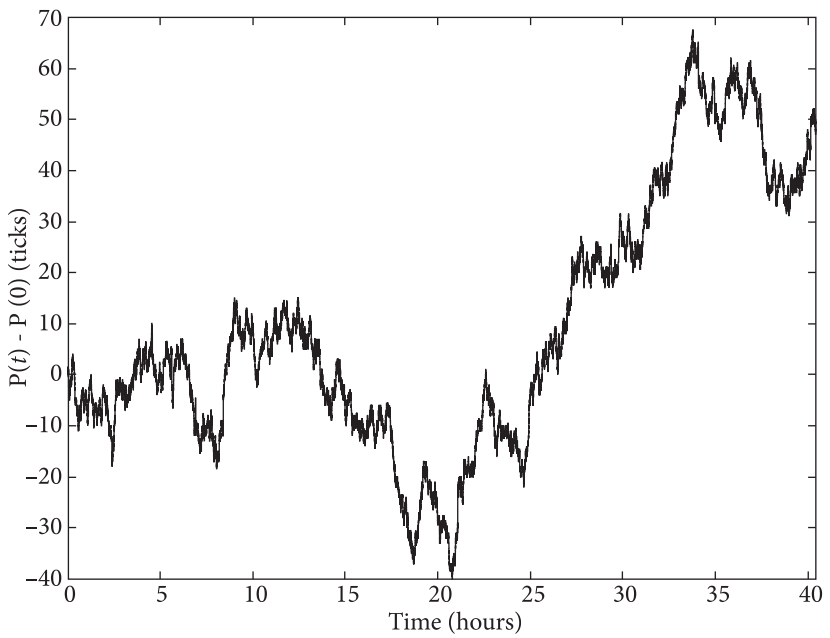

Fig. 9.6 Price sample path. At large time scales, the price process is close to a Wiener process. Extracted from Abergel and Jedidi (2013)

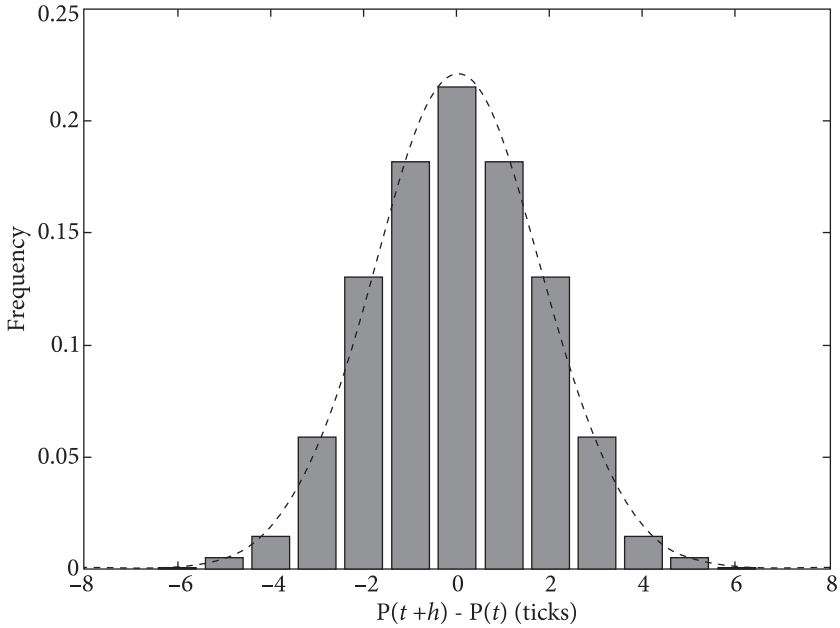

Fig. 9.7 Probability distribution of price increments. Time lag $h = 1000$ events. Extracted from Abergel and Jedidi (2013)

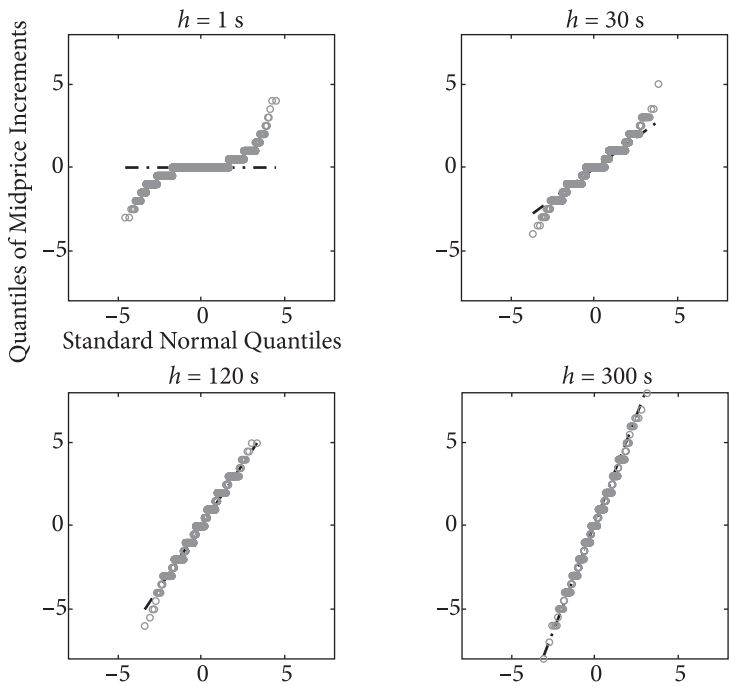

Fig. 9.8 Q-Q plot of mid-price increments. h is the time lag in seconds. This figure illustrates the aggregational normality of price increments. Extracted from Abergel and Jedidi (2013)

We now give a few facts on the properties of the variance of the price processes of our simulations. The *signature plot* of a price time series is defined as the variance of price increments at lag h normalized by the lag h, as a function of this lag h. In other words, it is the function $h \mapsto \sigma_h^2$ where

$$\sigma_h^2 = \frac{\mathbf{V}\left[P(t+h) - P(t)\right]}{h}. \tag{9.1}$$

This function measures the variance of price increments per time unit. Its main interest is that it shows the transition from the variance at small time scales where micro-structure effects dominate, to the long-term variance. Using the results of Chapter 6, in particular Theorem 6.5, one can show that

$$\lim_{h\to\infty} \sigma_h^2 = \sigma^2, \text{ for some fixed value } \sigma. \tag{9.2}$$

Figure 9.9 shows the signature plots computed on our simulations compared to the empirical ones. Signature plots are computed for both the trade prices and the mid-prices, and in both event and calendar time.

Two main observations are to be made. First, the simulated long-term variance is lower than the variance computed from the data. This observation remains valid for all CAC 40 stocks as documented in Fig. 9.10 Panel (c). We know that depth (shape) of the order book increases away from the best price towards the center of the book. In the absence of autocorrelation in trade signs, this would cause prices to wander less often far away from the current best as they hit a higher "resistance". We also suspect that actual prices exhibit locally more "drifting phases" than in our symmetric Markovian simulation where the expected price drift is null at all times. An interesting analysis of a simple order book model that allows time-varying arrival rates can be found in Challet and Stinchcombe (2003).

Second, the simulated signature plot is too high at short time scales relative to the asymptotic variance, especially for traded prices. As seen previously, this behaviour is well explained by the bid-ask bounce, which is too strong in the zero-intelligence model as there is no accounting for the clustering of orders of identical signs (see Subsection 9.2.4 below for a simple quantitative analysis of this phenomenon). It is however remarkable that the signature plot of empirical trade prices looks much flatter than the signature plot of simulated trade prices. Indeed, a flat empirical signature plot at all time scales suggests that the prices are actually diffusive, which seems to contradict the observation that empirical order signs exhibit positive long-ranged correlations. This has been observed and discussed in several empirical studies (Bouchaud et al. 2004; Lillo and Farmer, 2004; Farmer et al. 2006; Bouchaud et al. 2009). According to these studies, the paradox is solved by observing that the diffusivity results from two opposite effects:

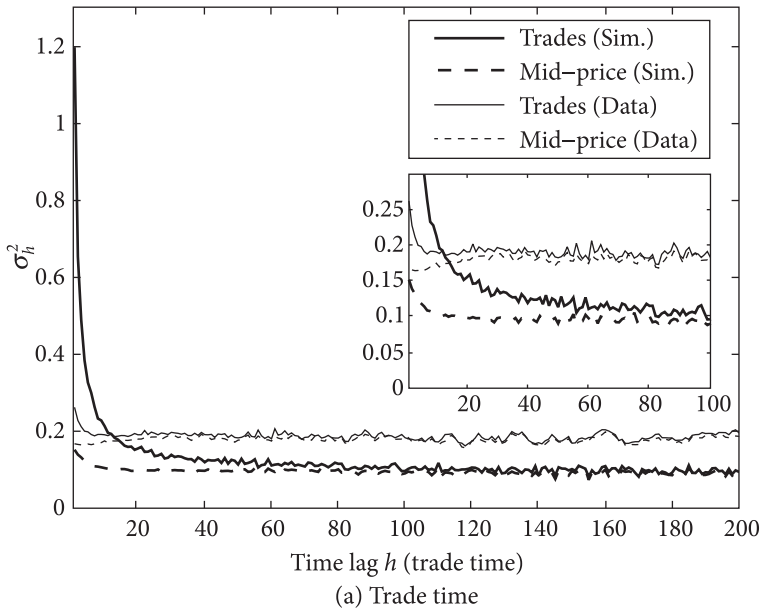

(a) Trade time

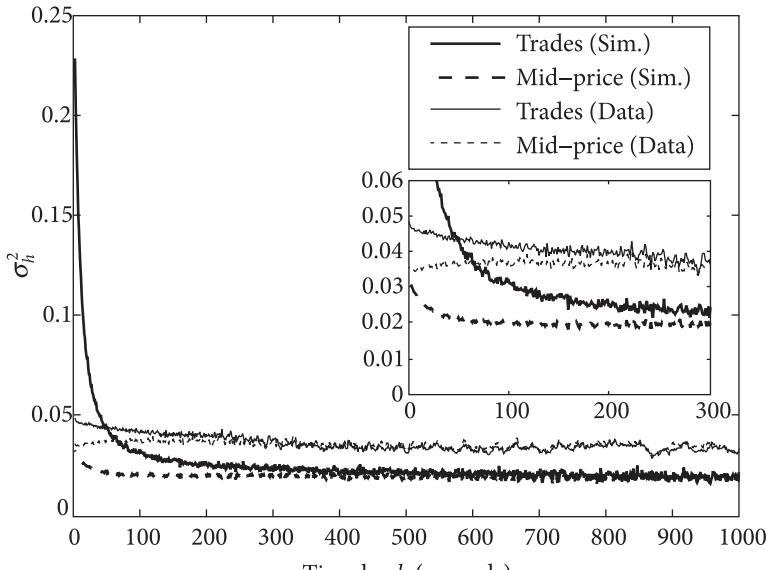

(b) Calendar time

Fig. 9.9 Signature plot: $\sigma_h^2 := \mathbb{V}\left[P(t+h) - P(t)\right]/h$. y axis unit is tick^2 per trade for panel (a) and tick^2. second^{-1} for panel (b). We used a 1,000,000 event simulation run for the model signature plots. Data signature plots are computed separately for each trading day $[9:30\text{–}14:00]$ then averaged across 23 days. For calendar time signature plots, prices are sampled every second using the last tick rule. The inset is a zoom-in. Extracted from Abergel and Jedidi (2013)

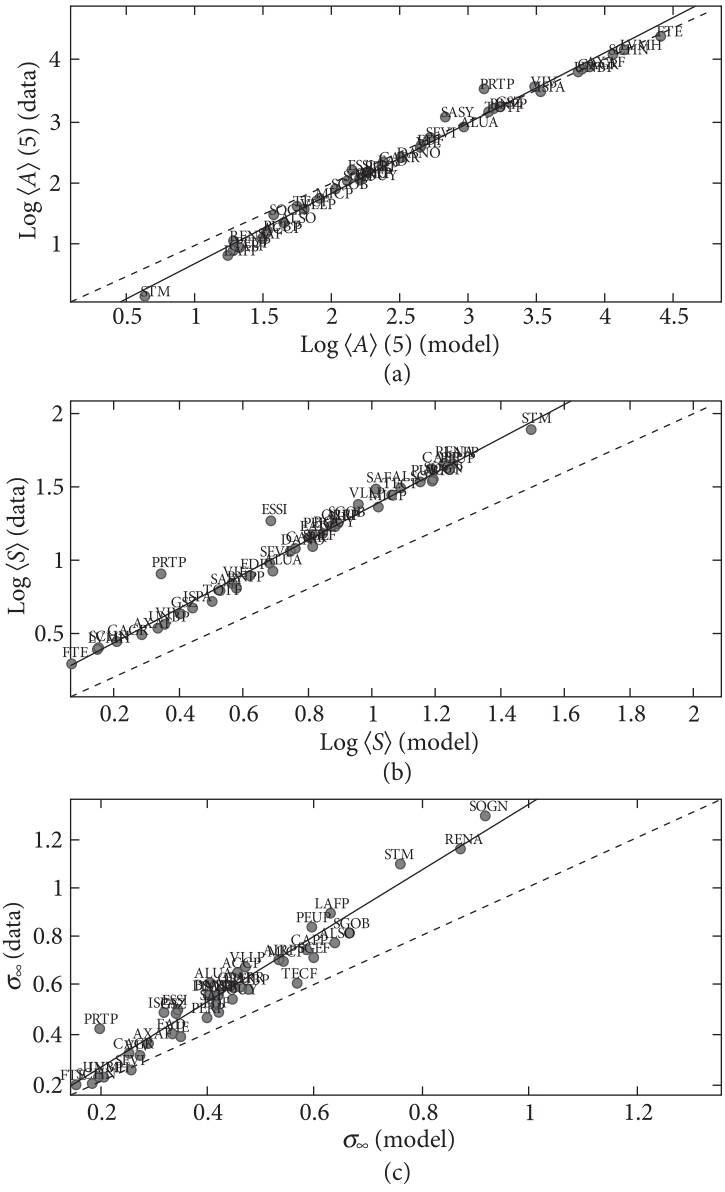

Fig. 9.10 A cross-sectional comparison of liquidity and price diffusion characteristics between the model and data for CAC 40 stocks (March 2011). Extracted from Abergel and Jedidi (2013)

On the one hand, autocorrelation in trade signs induces persistence in the price processes, while on the other hand, the liquidity stored in the order book induces mean-reversion. These two effects counterbalance each other exactly. This subtle equilibrium between liquidity takers and liquidity providers, which guarantees price diffusivity at short lags, is

not accounted for by the simple Poisson order book model that is simulated here, which explains our observations of anomalous diffusions at short time scales (see also Smith et al. 2003). Because of the absence of positive autocorrelation in trade signs in the model, this effect is magnified when one looks at trades. The next subsection elaborates on this point.

9.2.4 Anomalous diffusion at short time scales

We propose a heuristic argument for the understanding of the discrepancy between the model and the data signature plots at short time scales. In what follows, we use the trade time, i.e. the t-th trade occurs at time t. Denote by $P^{Tr}(t)$ the price of the trade at time t, and $\alpha(t)$ its sign:

$$\alpha(t) = \begin{cases} 1 & \text{for a buyer initiated trade, i.e. a buy market order,} \\ -1 & \text{for a seller initiated trade, i.e. a sell market order.} \end{cases}$$

We assume that the two signs are equally probable (symmetric model). But to make the argument valid for both the model (for which successive trade signs are independent) and the data (for which trade signs exhibit long memory) we do not assume independence of successive trade signs. Let $P(t^-)$ and $S(t^-)$ be the mid-price and spread just before the t-th trade. Then,

$$P^{Tr}(t) = P(t^-) + \frac{1}{2}\alpha(t)S(t^-). \tag{9.3}$$

For any process Z we define the increment $\Delta Z(t) = Z(t+1) - Z(t)$. With Eq. (9.3), the variance of the trade price process can be written:

$$\begin{aligned} \left(\sigma_1^{Tr}\right)^2 &= \mathbf{V}[\Delta P^{Tr}(t)] \\ &= \mathbf{E}\left[\left(\Delta P^{Tr}(t)\right)^2\right] \\ &= \mathbf{E}\left[\left(\Delta P(t^-)\right)^2\right] + \mathbf{E}\left[\Delta P(t^-)\Delta(\alpha(t)S(t^-))\right] + \frac{1}{4}\mathbf{E}\left[\left(\Delta(\alpha(t)S(t^-))\right)^2\right]. \end{aligned}$$

The first term in the right-hand side of the above equation is the variance of mid-price increments, denoted σ_1^2 thereafter. The second term represents the covariance of mid-price increments and the trade sign weighted by the spread. We may assume that this quantity is negligible. Indeed, this amounts to neglecting the correlation between trade signs and mid-quote movements, which can be justified by the dominance of cancellations and limit orders in comparison to market orders in order book data. We can thus focus on the third term and write:

$$\begin{aligned}\mathbf{E}\left[(\Delta(\alpha(t)S(t^-)))^2\right] &= \mathbf{E}\left[(\alpha(t+1)\Delta S(t^-) + S(t^-)\Delta\alpha(t))^2\right] \\ &= \mathbf{E}\left[(\Delta\alpha(t))^2\right]\mathbf{E}\left[S(t^-)^2\right] + 2\mathbf{E}\left[\alpha(t+1)\Delta S(t^-)S(t^-)\Delta\alpha(t)\right] \\ &\quad + \mathbf{E}\left[\alpha(t+1)^2\right]\mathbf{E}\left[(\Delta S(t^-))^2\right].\end{aligned}$$

Again, we neglect the cross term in the right-hand side, which amounts this time to neglect the correlation between trade signs and spread movements. We are thus left with:

$$\mathbf{E}\left[(\Delta(\alpha(t)S(t^-)))^2\right] \approx \mathbf{E}\left[(\Delta\alpha(t))^2\right]\mathbf{E}\left[S(t^-)^2\right] + \mathbf{E}\left[(\Delta S(t^-))^2\right].$$

Finally, if $\rho_1(\alpha)$ is the autocorrelation of trade signs at the first lag, we observe that:

$$\begin{aligned}\mathbf{E}\left[(\Delta\alpha(t))^2\right] &= \mathbf{E}\left[\alpha(t+1)^2\right] + \mathbf{E}\left[\alpha(t)^2\right] - 2\mathbf{E}\left[\alpha(t)\alpha(t+1)\right] \\ &= 2\left(1 - \rho_1(\alpha)\right),\end{aligned}$$

and we obtain:

$$\left(\sigma_1^{Tr}\right)^2 \approx {\sigma_1}^2 + \frac{1}{2}\left(1 - \rho_1(\alpha)\right)\mathbf{E}\left[S(t^-)^2\right] + \frac{1}{4}\mathbf{E}\left[(\Delta S(t^-))^2\right]. \tag{9.4}$$

More generally, a similar result after n trades may be written:

$$\left(\sigma_n^{Tr}\right)^2 \approx {\sigma_n}^2 + \frac{1}{2n}\left(1 - \rho_n(\alpha)\right)\mathbf{E}\left[S(t^-)^2\right]. \tag{9.5}$$

Two effects are clear from Eq. (9.4). First, the trade price variance at short time scales is larger than the mid-price variance. Second, autocorrelation in trade signs dampens this discrepancy. This explains at least partially why the trades signature plot obtained from the data is flatter than the model predictions: $\rho_1(\alpha)_{\text{model}} = 0$, while $\rho_1(\alpha)_{\text{data}} \approx 0.6$. Interestingly, although the arguments that led to (9.4) are rather qualitative, a back of the envelope calculation with $\mathbf{E}\left[S^2\right] \in [1, 9]$ gives a difference $\left(\sigma^{Tr}\right)^2 - \sigma^2$ in the range $[0.5, 4.5]$, which has the same order of magnitude of the values obtained by simulation.

From a modelling perspective, a possible solution to recover the diffusivity, even at very short time scales, is to incorporate long-ranged correlation in the order flow. Tóth et al. (2011) have investigated numerically this route using a "ϵ-intelligence" order book model. In this model, market orders signs are long-ranged correlated, that is, in trade time

$$\rho_n(\alpha) = \mathbf{E}\left[\alpha(t+n)\alpha(t)\right] \propto n^{-\gamma}, \qquad \gamma \in]0, 1[. \tag{9.6}$$

The size of incoming market orders is a fraction f of the volume displayed at the best opposite quote, with f drawn from the distribution

$$P_\xi(f) = \xi(1-f)^{\xi-1}, \tag{9.7}$$

It is shown in this model that by fine tuning the additional parameters γ and ξ, one can ensure a diffusive behaviour of the price both at a mesoscopic time scale (a few trades) and a macroscopic time scale (a few hundred trades)[2].

9.2.5 Results for CAC 40 stocks

In order to get a cross-sectional view of the performance of the model on all CAC 40 stocks, we estimate the parameters separately for each stock and run a 100,000 event simulation for each parameter set. We then compare in Figure 9.10 the average depth, average spread and the long-term "volatility" measured directly from the data, to those obtained from the simulations. Dashed line is the identity function. It would correspond to a perfect match between model predictions and the data. Solid line is a linear regression $z_{\text{data}} = b_1 + b_2\, z_{\text{model}}$ for each quantity of interest z. Parameters of the regression are given in Table 9.3.

We observe a good agreement between the average depth profiles (Panel (a)), and the model successfully predicts the relative magnitudes of the long-term variance σ_∞^2 and the average spread $\langle S \rangle$ for different stocks. However, it tends to systematically underestimate σ_∞^2 and $\langle S \rangle$. As explained above, this may be related to the absence of autocorrelation in order signs in the model and the presence of more drifting phases in empirical prices than in the simulated ones.

Table 9.3 CAC 40 stocks regression results

	b_1	b_2	R^2
$Log\,\langle A \rangle\,(5)$	$-0.42\ (\pm 0.11)$	$1.13\ (\pm 0.04)$	0.99
$Log\,\langle S \rangle$	$0.20\ (\pm 0.06)$	$1.16\ (\pm 0.07)$	0.97
σ_∞	$-0.012\ (\pm 0.05)$	$1.35\ (\pm 0.11)$	0.94

9.3 Simulation of a Limit Order Book Modelled by Hawkes Processes

The basic order book simulator is now enhanced with arrival times of limit and market orders following mutually exciting Hawkes processes, as in the model described and

[2]Note that Toth. el al. Tóth et al. (2011) model the "latent order book", not the actual observable order book. The former represents the *intended* volume at each price level p, that is, the volume that would be revealed should the price come close to p. So that the interpretation of their parameters, in particular the expected lifetime τ_{life} of an order, does not strictly match ours.

mathematically analysed in Chapter 8. We present numerical procedures for the estimation and simulation of Hawkes processes. We show in Section 9.3.4 that using Hawkes process-driven order flows enables a more realistic behaviour of the bid-ask spread than Poissonian order flows.

9.3.1 Simulation of the limit order book in a simple Hawkes model

It is known [Large (2007) Da Fonseca and Zaatour (2014b)] that there is a strong clustering of the arrivals of market and limit orders, and we have also seen in Chapter 4 that the flow of limit orders strongly interact with the flow of market order. Such observations naturally advocate for the use of Hawkes processes to model the intensities of submissions of market and limit orders, as was already presented and mathematically studied in Chapter 8.

In this section, we analyze a low-dimensional Hawkes process-based limit order book model. Flows of limit and market orders are represented by two Hawkes processes N^L and N^M, with stochastic intensities respectively λ^L and λ^M defined as:

$$\lambda^M(t) = \lambda_0^M + \int_0^t \alpha_{MM} e^{-\beta_{MM}(t-s)} dN_s^M,$$
$$\lambda^L(t) = \lambda_0^L + \int_0^t \alpha_{LM} e^{-\beta_{LM}(t-s)} dN_s^M + \int_0^t \alpha_{LL} e^{-\beta_{LL}(t-s)} dN_s^L.$$

Three mechanisms can be used here. The first two are self-exciting ones, MM and LL. They are a way to translate into the model the observed clustering of arrival of market and limit orders and the broad distributions of their durations. The third mechanism, LM, is the direct translation of the *market making* property we have identified in Chapter 4. When a market order is submitted, the intensity of the limit order process N^L increases, enforcing the probability that the next event will illustrate a market making behaviour. Note that, for the sake of computational simplicity, we do no implement the reciprocal mutual excitation ML: Although a *market taking* effect has been identified in Chapter 4, it was not observed with all limit orders, but only with the aggressive ones. Since, we preferred to keep the model low-dimensional, the ML effect is not implemented here. Some calibration results based on a more complete model including the market taking effect will be presented in Section 9.4.

9.3.2 Algorithm for the simulation of a Hawkes process

We now have to modify our routine for the simulation of a limit order book with Poissonian order flows (Algorithm 1) and replace the simulation of events with exponentially distributed inter-event times (lines 4 and 5 of the algorithm) with the simulation of the Hawkes processes N^M and N^L.

Below is a generic algorithm that simulates a P-variate Hawkes process with intensities

$$\lambda^n(t) = \lambda_0^n(t) + \sum_{m=1}^{P} \int_0^t \alpha_{nm} e^{-\beta_{nm}(t-s)}\, dN^m(s), \quad n = 1, \dots P$$

The simulation is based on a *thinning* method (Lewis and Shedler, 1979). Let $[0, T]$ be the time interval on which the process is to be simulated. We define $I^K(t) = \sum_{n=1}^{K} \lambda^n(t)$ the sum of the intensities of the first K components of the multivariate process. $I^P(t) = \sum_{n=1}^{P} \lambda^n(t)$ is thus the total intensity of the multivariate process and we set $I^0 = 0$.

The detailed routine is given in Algorithm 2.

Algorithm 2 Generic thinning algorithm for the simulation of a multivariate Hawkes process.

Require: Deterministic base intensities $\lambda^n(t)$ and exponential kernel parameters (α_{mn}) and (β_{mn}), $m, n = 1, \dots, P$ for the P-variate Hawkes process.

1: **Initialization**: Set $i^1 \leftarrow 1, \dots, i^P \leftarrow 1$ and $I^* \leftarrow I^P(0) = \sum_{n=1}^{P} \lambda_0^n(0)$.

2: **Time of first event**: Draw s exponentially distributed with parameter I^*.

3: **while** $s < T$

4: Draw D uniformly distributed on $[0, 1]$.

5: **if** $D \leq \frac{I^P(s)}{I^*}$ **then**

6: Set $t_{i^{n_0}}^{n_0} \leftarrow s$ where n_0 is such that $\frac{I^{n_0-1}(s)}{I^*} < D \leq \frac{I^{n_0}(s)}{I^*}$. (New event of type n_0)

7: Set $i^{n_0} \leftarrow i^{n_0} + 1$.

8: **end if**

9: **Update maximum intensity**: Set $I^* \leftarrow I^P(s)$. I^* exhibits a jump of size $\sum_{n=1}^{P} \alpha_{nn_0}$ if an event of type n_0 has just occurred.

10: **Time of next event**: Draw s exponentially distributed with parameter I^*.

11: **end while**

Ensure: $\left(\{t_i^n\}_i\right)_{n=1,\dots,P}$ is a sample path of a multivariate Hawkes process on $[0, T]$.

As an illustration we provide some examples of simulations of bivariate Hawkes processes using Algorithm 2. Figure 9.11 shows an example of such a simulation for parameters, and Fig. 9.12 zooms in on a small part of this simulation. Parameters used to compute these graphs are:

$$\lambda_0^1 = 0.1, \alpha_1^{11} = 0.2, \beta_1^{11} = 1.0, \alpha_1^{12} = 0.1, \beta_1^{12} = 1.0,$$
$$\lambda_0^2 = 0.5, \alpha_1^{21} = 0.5, \beta_1^{21} = 1.0, \alpha_1^{22} = 0.1, \beta_1^{22} = 1.0, \tag{9.8}$$

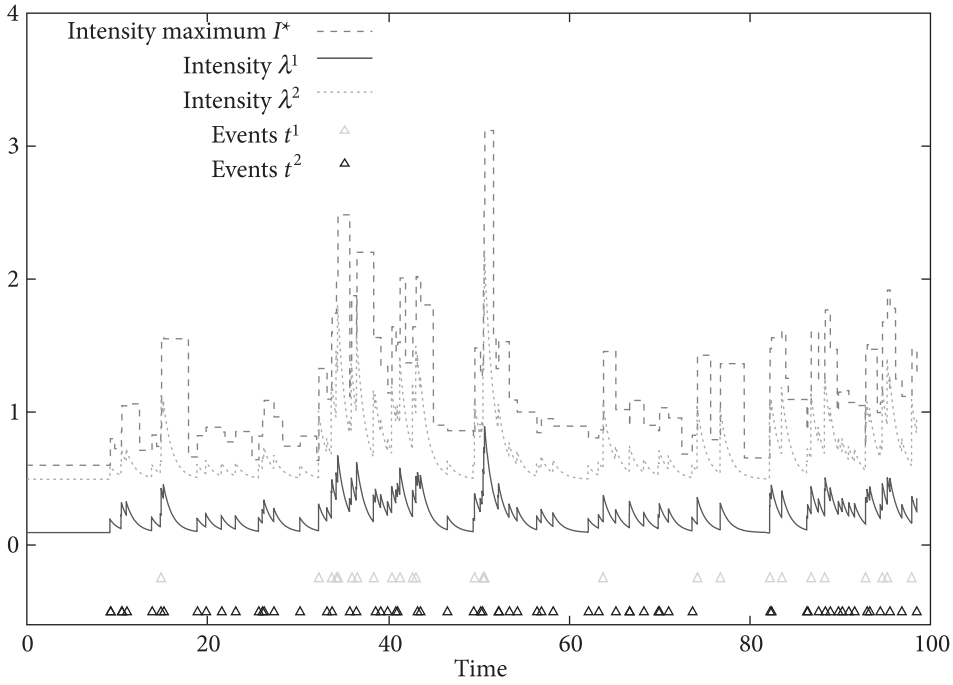

Fig. 9.11 Simulation of a two-dimensional Hawkes process with parameters given in Eq. (9.8)

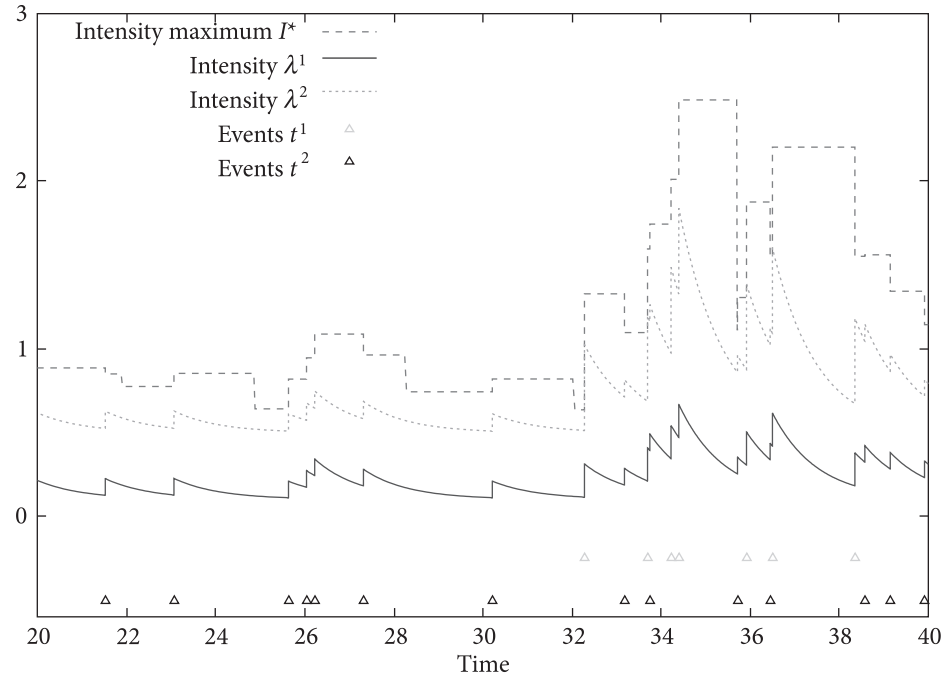

Fig. 9.12 Simulation of a two-dimensional Hawkes process parameters given in Eq. (9.8). (Zoom of Fig. 9.11)

9.3.3 Parameter estimation

The Hawkes model described above has many variants: By forcing some αs to be zero, we can turn off one or several of these features. We therefore have several models to test: namely LM, MM, MM + LM, MM + LL, MM + LL + LM – and try to understand the influence of each effect. As a reference, we will also simulate the model in which N^M and N^L are homogeneous Poisson processes. This variant will be referred to as HP.

Hawkes processes can be estimated by a maximum likelihood method. Details for an efficient computation of the log-likelihood are given in Appendix C.1.1. We fit both N^L and N^M processes by computing on our data these maximum likelihood estimators of the parameters of the different variants of the model. As expected, estimated values varies with the market activity on the day of the sample. However, it appears that estimation of the parameters of stochastic intensity for the MM and LM effect are quite robust. We find an average relaxation parameter $\hat{\beta}_{MM} = 6$, i.e. roughly 170 milliseconds as a characteristic time for the MM effect, and $\hat{\beta}_{LM} = 1.8$, i.e. roughly 550 milliseconds characteristic time for the LM effect. Estimation of models including the LL effect are more troublesome on our data. In the simulations that follows, we assume that the self-exciting parameters are similar ($\alpha_{MM} = \alpha_{LL}$, $\beta_{MM} = \beta_{LL}$) and ensure that the number of market orders and limit orders in the different simulations is roughly equivalent (i.e. approximately 145000 limit orders and 19000 market orders for 24 hours of continuous trading). Table 9.4 summarizes the numerical values used for simulation. Fitted parameters are in agreement with an assumption of asymptotic stationarity. We compute long runs of simulations with our enhanced model, simulating each time 24 hours of continuous trading. With these parameters, the order book is never empty during the simulations. Note however that there is no mechanism to prevent the limit order book from becoming empty. If needed, one can enforce the limits a_∞ and b_∞ for some price far away from the best prices, as in Algorithm 1. Statistics based on the simulation results are discussed in the Section 9.3.4.

Table 9.4 Estimated values of parameters used for simulations

Model	μ_0	α_{MM}	β_{MM}	λ_0	α_{LM}	β_{LM}	α_{LL}	β_{LL}
HP	0.22	-	-	1.69	-	-	-	-
LM	0.22	-	-	0.79	5.8	1.8	-	-
MM	0.09	1.7	6.0	1.69	-	-	-	-
MM LL	0.09	1.7	6.0	0.60	-	-	1.7	6.0
MM LM	0.12	1.7	6.0	0.82	5.8	1.8	-	-
MM LL LM	0.12	1.7	5.8	0.02	5.8	1.8	1.7	6.0

Common parameters:	$m_1^P = 2.7, \nu_1^P = 2.0, s_1^P = 0.9$ $m_1^V = 275, m_2^V = 380$ $\lambda^C = 1.35, \delta = 0.015$

9.3.4 Performances of the simulation

In this section, we present the results of the simulation of the Hawkes process-based model described above. Other than the arrival times of events, there are some differences with the order book simulation described in Algorithm 1: first, the volume distributions $\mathcal{V}^M$ and $\mathcal{V}^L$ are exponential (instead of Log-Gaussian). Second, we do not keep track of the intensities λ_i^L for each price level i, but use instead one process N^L for the submission of limit order. The submission price of an incoming limit orders is then drawn according to a parametric (Student) distribution centred around the same side best quote and truncated at the opposite best price. Third, the size of these new limit orders is randomly drawn according to an exponential distribution with mean m_L^V.

These are minor changes implemented in order to study some alternatives to the choices in Section 9.2, but their influence on the results we present here is clearly moderate, the empahsis being on the arrival times.

With these specifications, we have the following results. Firstly, we can easily check that introducing self- and mutually exciting processes into the order book simulator helps producing more realistic arrival times. Figure 9.13 shows the distributions of the durations of market orders (left) and limit orders (right). As expected, we check that the Poisson assumption has to be discarded, while the use of Hawkes processes helps give more weight to very short time intervals. We also verify that models with only self-exciting processes MM and LL are not able to reproduce the market making feature described in Chapter 4. Distribution of time intervals between a market order and the next limit order are plotted on Fig. 9.14. As expected, no peak for short times is observed if the LM effect is not in the model. However, when the LM effect is included, the simulated distribution of time intervals between a market order and the following limit order is very close to the empirical one.

Besides offering a better simulation of the arrival times of orders, we argue that the LM effect also helps simulating a more realistic behaviour of the bid-ask spread of the order book. On Fig. 9.15, we compare the distributions of the spread for three models – HP, MM, MM+LM – with respect to the empirical measures. We first observe that the model with homogeneous Poisson processes produces a fairly good shape for the spread distribution, but slightly shifted to the right. Small spread values are largely underestimated. When adding the MM effect in order to get a better grasp at market orders' arrival times, it appears that we flatten the spread distribution. One interpretation could be that when the process N^M is excited, markets orders tend to arrive in cluster and to hit the first limits of the order book, widening the spread and thus giving more weight to large spread values. However,

since the number of orders is roughly constant in our simulations, there has to be periods of lesser market activity where limit orders reduce the spread. Hence, a flatter distribution. The MM + LM model produces a spread distribution much closer to the empirical shape. It appears from Fig. 9.15 that the LM effect reduces the spread: the market making behaviour helps giving less weight to larger spread values (see the tail of the distribution) and to sharpen the peak of the distribution for small spread values.

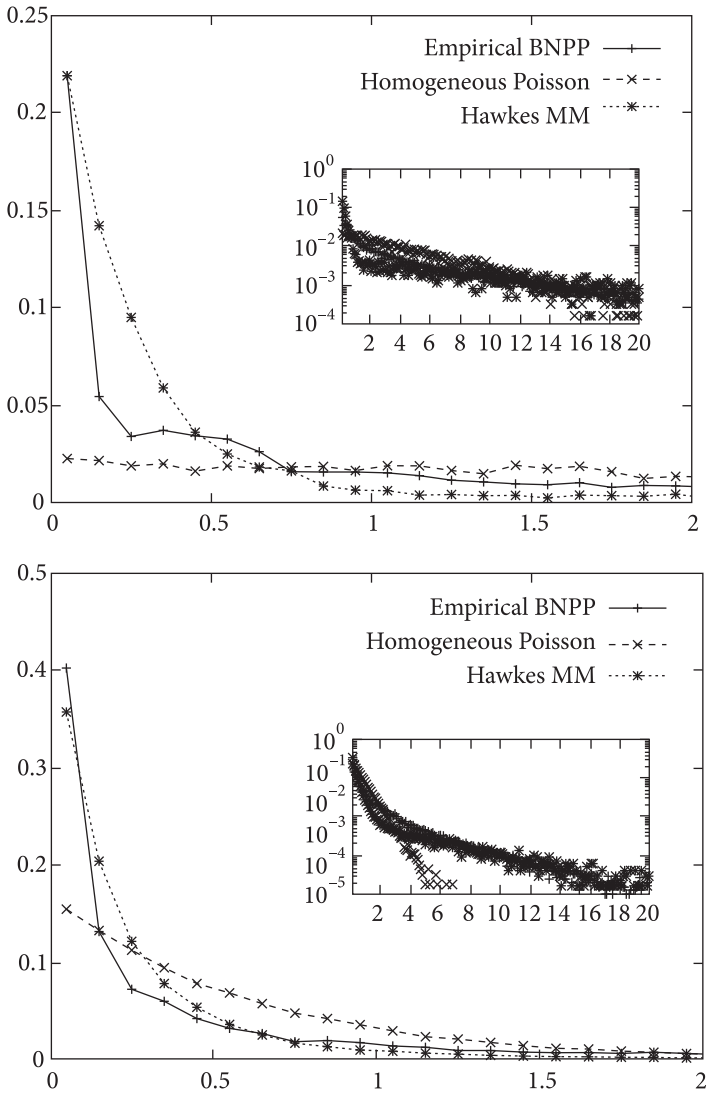

Fig. 9.13 Empirical density function of the distribution of the durations of market orders (left) and limit orders (right) for three simulations, namely HP, MM, LL, compared to empirical measures. In inset, same data using a semi-log scale. Extracted from Muni Toke (2011)

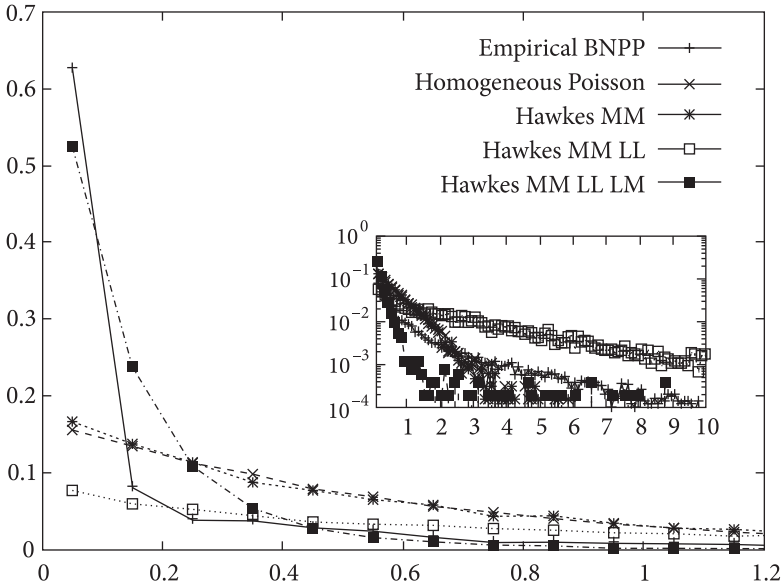

Fig. 9.14 Empirical density function of the distribution of the time intervals between a market order and the following limit order for three simulations, namely HP, MM+LL, MM+LL+LM, compared to empirical measures. In inset, same data using a semi-log scale. Extracted from Muni Toke (2011)

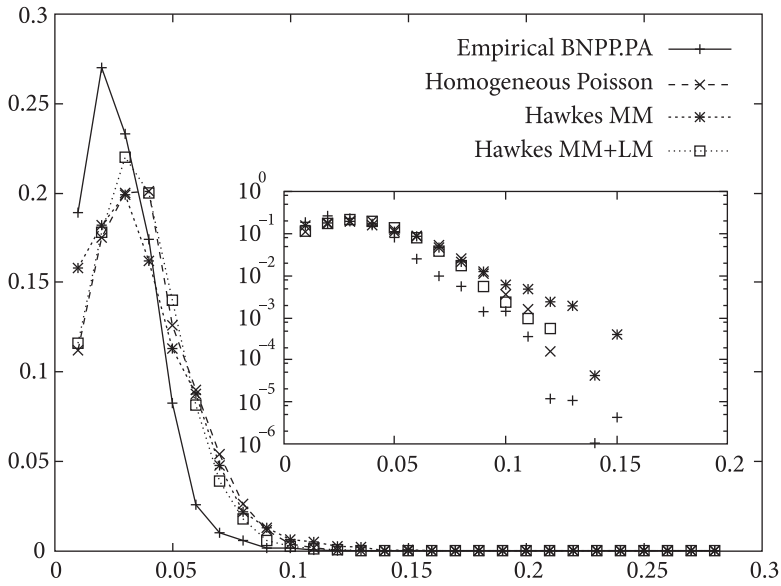

Fig. 9.15 Empirical density function of the distribution of the bid-ask spread for three simulations, namely HP, MM, MM+LM, compared to empirical measures. In inset, same data using a semi-log scale. X-axis is scaled in euro (1 tick is 0.01 euro). Extracted from Muni Toke (2011)

We show on Fig. 9.16 that the same effect is observed in an even clearer way with the MM + LL and MM + LL + LM models.

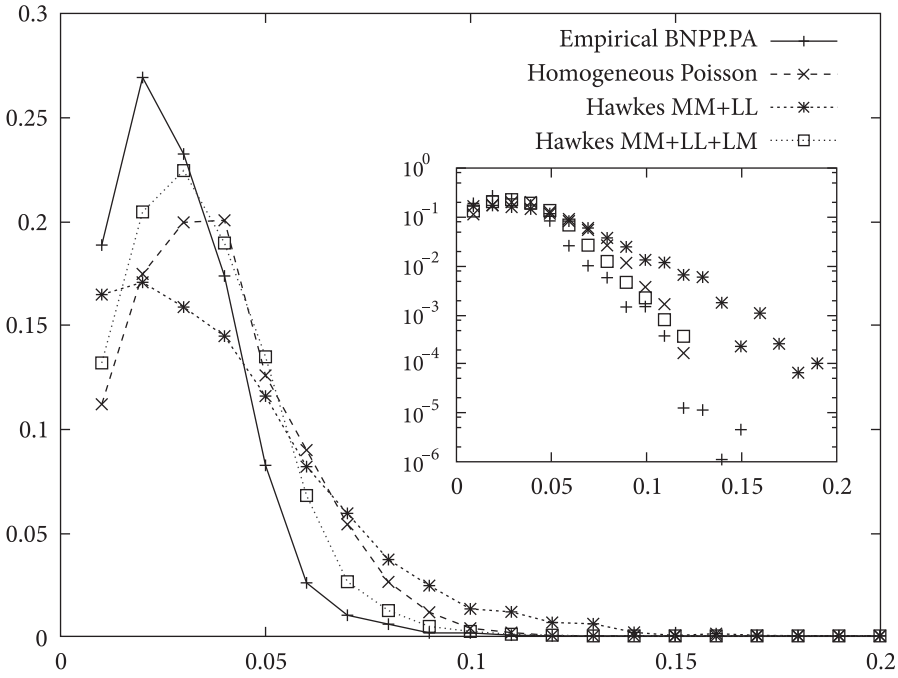

Fig. 9.16 Empirical density function of the distribution of the bid-ask spread for three simulations, namely HP, MM, MM + LM, compared to empirical measures. In inset, same data using a semi-log scale. X-axis is scaled in euro (1 tick is 0.01 euro). Extracted from Muni Toke (2011)

Actually, the spread distribution produced by the MM + LL model is the flattest one. This is in line with our previous argument. When using two independent self exciting Hawkes processes for arrival of orders, periods of high market orders' intensity gives more weight to large spread values, while periods of high limit orders' intensity gives more weight to small spread values. Adding the cross-term LM to the processes implements a coupling effect that helps reproducing the empirical shape of the spread distribution. The MM + LL + LM simulated spread is the closest to the empirical one.

Finally, it is somewhat remarkable to observe that these variations of the spread distributions are obtained with little or no change in the distributions of the variations of the mid-price. As shown on Fig. 9.17, the distributions of the variations of the mid-price sampled every 30 seconds are nearly identical for all the simulated models.

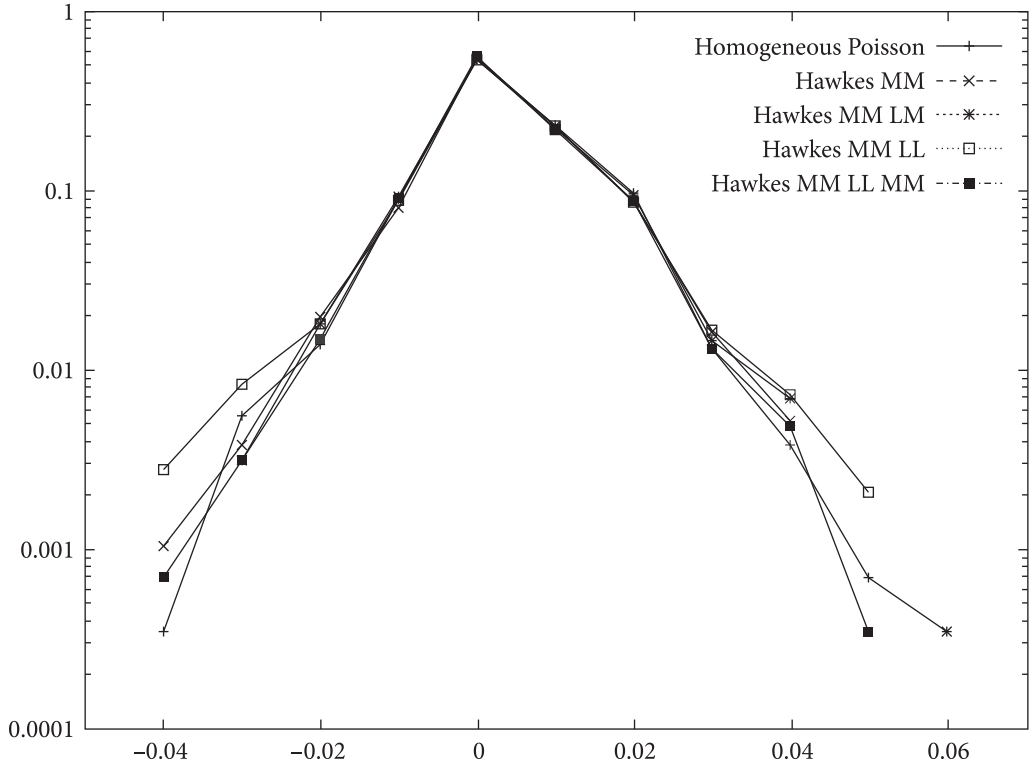

Fig. 9.17 Empirical density function of the distribution of the 30-second variations of the mid-price for five simulations, namely HP, MM, MM+LM, MM+LL, MM+LL+LM, using a semi-log scale. X-axis is scaled in euro (1 tick is 0.01 euro). Extracted from Muni Toke (2011)

9.4 Market Making and Taking, Viewed from a Hawkes-process Perspective

In this short section, we analyze the calibration results of a more general Hawkes process-based model for the limit order book. This time, we distinguish between limit (L) and market (M) orders that change the price (denoted A for aggressive) and those that do not change the price (denoted P for passive); hence we consider four types of orders, denoted by the abbreviations AM, PM, AL and PL. These four types of events are modelled with a four-dimensional Hawkes process $N(t) = (N^{AM}(t), N^{PM}(t), N^{AL}(t), N^{PL}(t))$ with a constant base intensity and an exponential kernel. In other words, the process N has the intensity $\boldsymbol{\lambda}(t) = (\lambda^{AM}(t), \lambda^{PM}(t), \lambda^{AL}(t), \lambda^{PL}(t))$ satisfying:

$$\boldsymbol{\lambda}(t) = \boldsymbol{\lambda}_0 + \int_0^t K(t-u)dN(u), \tag{9.9}$$

where $\boldsymbol{\lambda}_0 = (\lambda_0^{AM}, \lambda_0^{PM}, \lambda_0^{AL}, \lambda_0^{PL})$ is the base intensity and the kernel matrix K has general term $K_{ij}(u) = \alpha_{ij} e^{-\beta_{ij} u}$, $i, j \in \{AM, PM, AL, PL\}$. As before, the model is fitted to the data using a maximum-likelihood estimation described in Appendix C.1.1. In this example, we use 14 days of trading (February 1st to 23rd, 2010) for twelve randomly selected CAC 40 stocks traded on the Paris Bourse. Since, the empirical results in Chapter 4, Section 4.4.1 section has exhibited, as expected, a certain symmetry between the bid and ask sides, we do not distinguish the buy and sell sides and merge all events of the same type from both the bid and ask sides of the book. Following Large (2007), we visualize the results by plotting circles with center coordinates $(\alpha_{ij}, \ln(2)\beta_{ij}^{-1})$ and a diameter proportional to the number of exciting events j. Thus, the higher the circle, the stronger the influence of the corresponding event. Similarly, circles on the right side of the graph have a longer influence.

Figure 9.18 plots for the twelve stocks the resulting circles for events that influence the intensity of aggressive limit orders (parameters α_{AL-j} and β_{AL-j}).

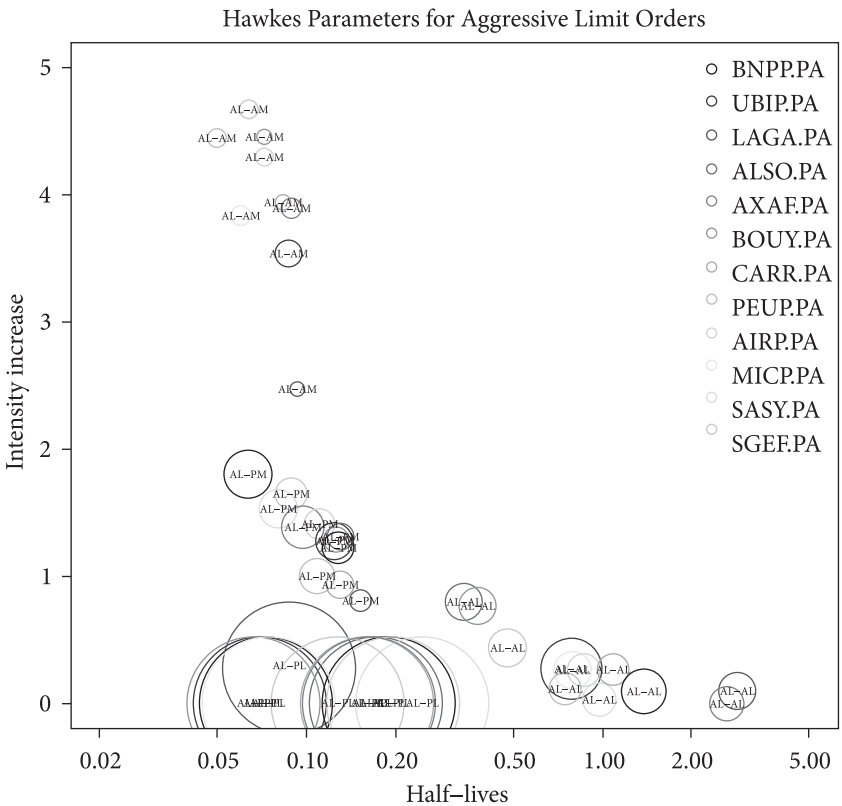

Fig. 9.18 Hawkes parameters for aggressive limit orders for various CAC40 stocks. These values are computed using MLE estimation on 14 days of trading (Feb.1st-Feb.23rd 2010), 10am-12pm

The intensity of the arrival process of limit orders submitted inside the spread is strongly excited by aggressive market orders, with a rather short half-life. We thus observe here a return of liquidity that tightens the spreads after its widening by an aggressive market order: This is the market making effect already described. Another similar effect of resilience in the order book is observed, a bit less strongly, with passive market orders. The third notable influence is due to the aggressive limit orders, with a less intense effect but longer half-life, illustrating the clustering of these aggressive limit orders. The limited effect of passive limit orders appears in contrast negligible. It is important to remark that this pattern is a general one: All circles of the same type are grouped together on the same part of the graph, i.e. each of the 12 studied stocks exhibit roughly the same behaviour with respect to clustering and market making.

Regarding the reciprocal excitations on aggressive market orders, results are presented on Fig. 9.19.

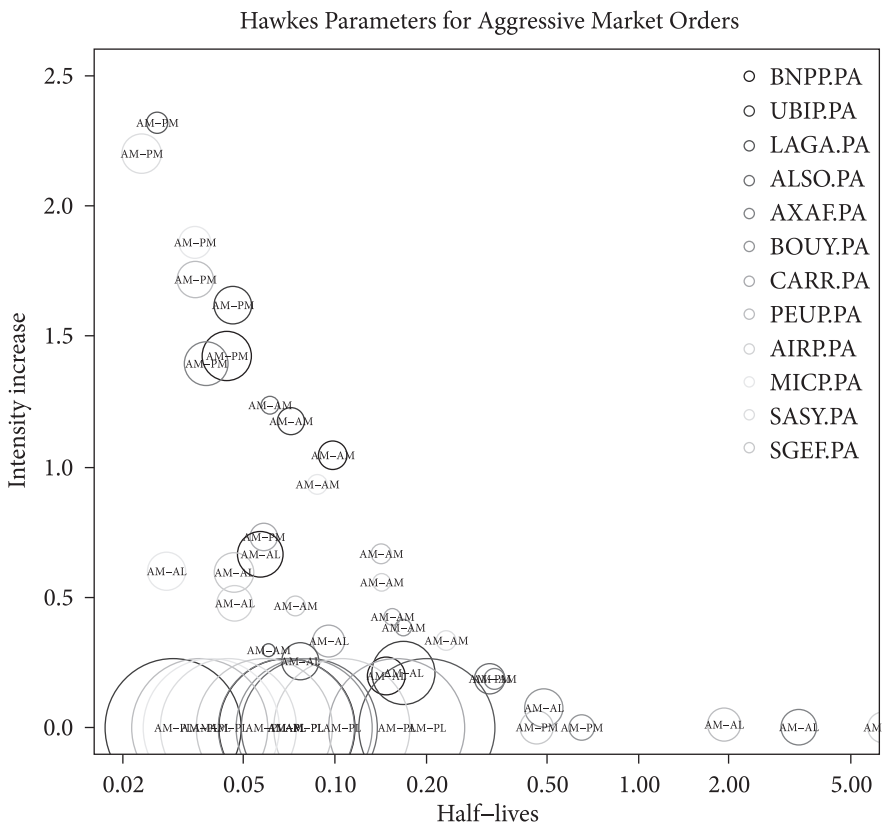

Fig. 9.19 Hawkes parameters for aggressive market orders for various CAC40 stocks. These values are computed using MLE estimation on 14 days of trading (Feb.1st-Feb.23rd 2010), 10am-12pm

The intensity of the arrival process of market orders that move the price is strongly excited by passive and aggressive market orders. This is an illustration of the clustering of trades, and possibly of a rush to decreasing liquidity: When the volume available at the best limit decreases due to several passive market orders, an aggressive market order is likely to quickly take the remaining liquidity. We also observe a clear influence of aggressive limit orders on aggressive market orders, which corresponds to a market taking effect. This is in line with the observations of Section 4.4.1 based on the use of lagged correlation coefficients. It is however interesting to remark that the strength and length of this effect varies across the stocks studied, i.e. the patterns are less clearly defined for the influence on aggressive market orders than they were in the previous case for the influence of aggressive limit orders.

9.5 Conclusion

This chapter was primarily motivated by practical considerations: when using a particular limit order book model, it is important to assess its reliability in reproducing the behaviour of real markets.

Starting with the basic zero-intelligence paradigm and progressing towards more refined models based on Hawkes processes, we have studied limit order book models that can be used to benchmark market making or statistical arbitrage strategies. Note that we do not present results on general state-dependent intensities in this work, and refer the interested reader to some recent contributions such as Huang et al. (2015).

In a different but related direction, a very general, flexible open-source library has been developped by A. Kolotaev in the Chair of Quantitative Finance, and can be found at http://fiquant.mas.ecp.fr. Its purpose is to provide a generic framework for the study of trading strategies in order-driven markets.